5 JET Notifications

JET Notifications

- Laser detritiation and co-deposit removal for various plasma-facing components supported by optical spectroscopy and ion diagnostics
- Assessment of efficiency of laser removal of fuel-inventory for mixed material samples using LIBS
- Assessment of the suitability of neutron and gamma detectors in the future experiment at JET for the validation of shutdown dose rate prediction
- MCNP simulation for JET 3U irradiation–end
- Gamma Ray Cameras: Neutron Attenuators
- Gas Electron Multiplier Detector for X-ray Crystal Spectrometry – GXS
- Impurity production from the ICRH antennae in JET

Laser detritiation and co-deposit removal for various plasma-facing components supported by optical spectroscopy and ion diagnostics

Corresponding author **Monika Kubkowska**
monika.kubkowska@ipplm.pl

The goal of the task was investigation of laser removal of co-deposited layers from various plasma facing components from tokamaks and calibrated samples containing JET/ITER relevant materials. The samples which were under investigation in the framework of the task were components of tokamak limiters and divertors. The components were previously installed in the operating machines (TEXTOR, AUG) and were subjected to the tokamak plasma which led to erosion/deposition on their surface. The research at the 1PPLM were aimed both on laser removal of the deposited layers and on characterization of the surface of the components. In addition calibrated samples containing JET-like materials provided by collaborating institutes were under investigation.

As diagnostic techniques for surface investigation and characterization of the removal process there were applied real-time methods such as LIBS (Laser Induced Breakdown Spectroscopy) and ion diagnostics (ion collectors and electrostatic ion energy analyzer).

For the AUG samples the experiments with electrostatic ion energy analyzer (IEA) gave consistent results with LIBS and confirmed removal of the fuel-containing thin co-deposit layer. The results from IEA moreover showed the presence of some amounts of carbon contamination in the tungsten layer. It should be noted that the IEA is a device of very high sensitivity and the observed carbon signal may at least partly be contributed by material deposited on the laser treated surface between laser shots.

The results of the IEA were consistent with the results of LIBS which also indicated presence of deuterium in the surface of the samples. The deuterium can be seen only in first two shots where its magnitude is high enough to dominate over all other lines in its neighborhood.

Integration of the lines allowed for estimation of the depth profile of the samples. A representative one is given in figure 1. For this estimation lines from another spectral range was used (426-432 nm) due to higher intensity of the W and C lines and better S/N ratio representative for that region.

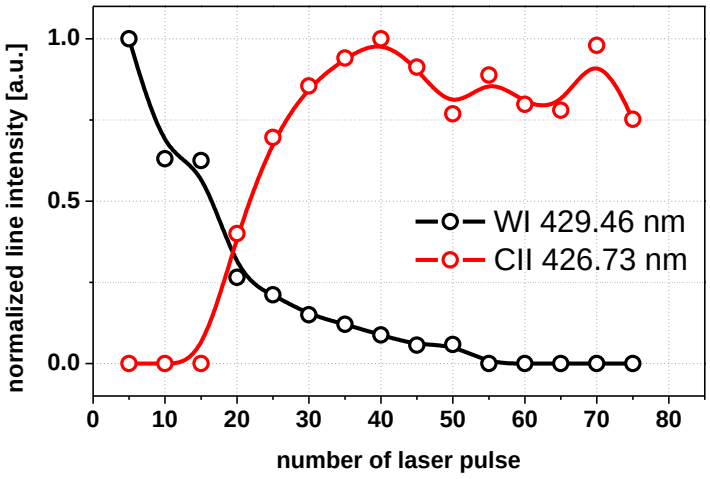

Fig. 1. Spectroscopy-based depth profile of an A UG divertor sample

In the case of the removal of the thick co-deposit from the TEXTOR limiter sample there was a need to deposit significantly higher number of shots to remove the fuel containing layer. The process of removal recorded by the LIBS system for such a sample is presented in figure 2.

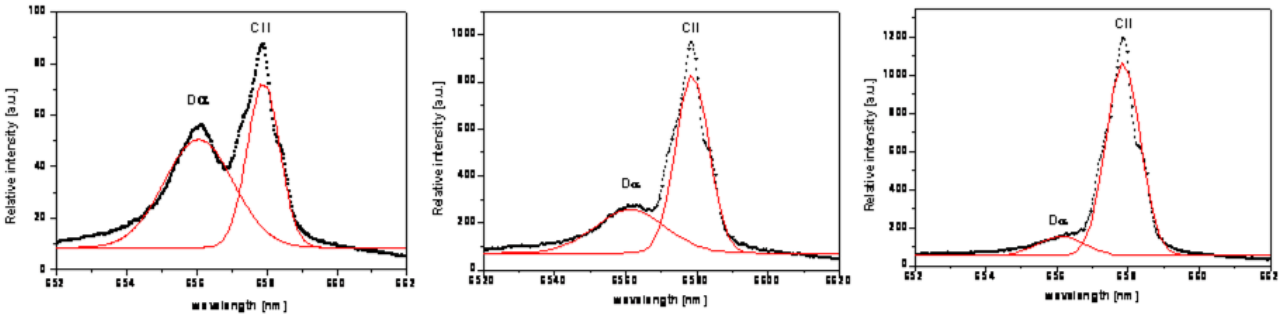

Fig. 2. Illustration of the removal the deposit from the TEXTOR limiter sample – spectra for 5, 20 and 40 shots, respectively

The whole spectra obtained at the beginning and after the removal process are presented in figure 3. As it can be seen, the spectra look stable and line identification is relatively easy. In the spectrum on the left (before removal) the deuterium line can be clearly seen while it is completely absent in the spectrum on the right (after removal).

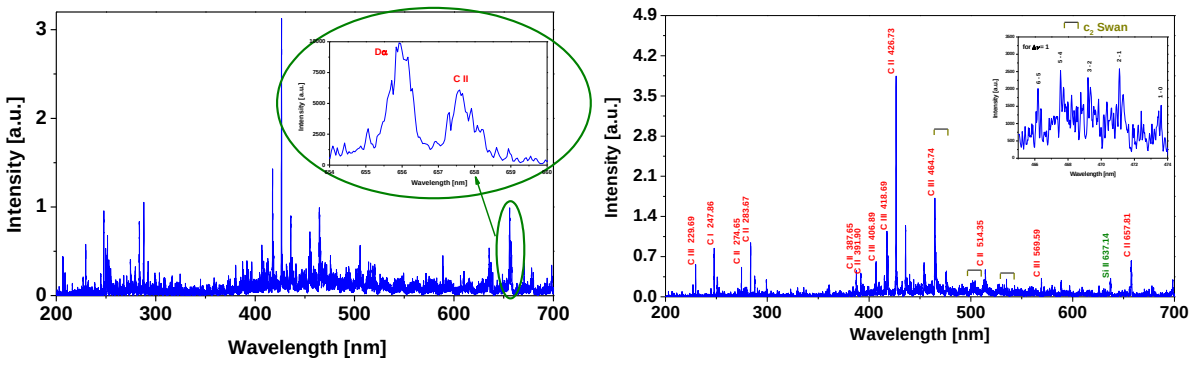

Fig. 3. The whole spectrum taken for the TEXTOR sample before laser irradiation (left) and after deposition of 40 laser shots (right)

Promising results were also obtained in tests of the fiber laser for fuel removal. First experiments used Yb:fiber (100 kHz rep. rate. 100 ns pulses of 1 mJ) as a irradiation source for removal and Nd:YAG pulses as a source for generation of plasma for LIBS before and after the irradiation by the fiber laser. The results clearly indicate that after 1 s irradiation by the fiber laser, the fuel particles were completely removed from the target surface. Another experiment with Yb:fiber laser was conducted to test a possibility of "dustless" fuel removal. For that purpose a cylindrical aluminum dust collector (which was used in previous experiments at IPPLM) was mounted in front of the target plate. The collector has a drilled top to transmit the fiber beam with a ability to collect most of the dust generated during the interaction process. In previous experiments dust was successfully collected in this way in form of both macroscopic particles and deposited on its walls in a film of microscopic/nano particles and was investigated in collaborating laboratories. In the preliminary experiment with fiber laser no macroscopic particles of dust were found in the collector which may indicate that the removal process with this laser can lead to removal without further fuel retention in dust particles released during the process. It may result from less rapid character of the phenomena of laser-matter interaction in the regime of lower power densities. In the case of the fiber laser the particles are mostly released by the mechanism of thermal desorption, whereas in the regime of high power density provided by a q-switched Nd:YAG laser the mechanisms of laser ablation and brittle destruction dominate.

The research on the task fruited in demonstration of effective application of the LIBS method in mixed material conditions both for samples taken from a real machine and for calibrated samples. Observation of the spectral lines in a narrow band which was representative for all chemical components present in spectra simplified the interpretation of results and effectively improved the rate on which the spectra could have been recorded (from 0.5 Hz when full wavelength range spectra were collected to 2 Hz for a narrow band from 426 to 432 nm).

Another interesting finding which was gained in the research on mixed materials is a strong influence not only of the chemical composition but also of the origin of the laser treated surfaces on the removal rate. For example removal rate of the layer of C:W which was prepared by magnetron sputtering was at the level of 0.7 nm per laser shot which was significantly larger than me one obtained for pure tungsten layer on AUG samples (~0.2um).

Possibility of efficient fuel removal without dust production with a use of high power fiber laser which has been demonstrated this year may appear to be a very reasonable alternative for this task among other candidate methods. The development of the fiber laser application undoubtedly should be in the scope of future research.

At the end, it is worthwhile to add that the reported task (JW9-NFT-POL-04) has been finalized and the report was accepted by EFDA.

Assessment of efficiency of laser removal of fuel-inventory for mixed material samples using LIBS

Corresponding author **Monika Kubkowska**
monika.kubkowska@ipplm.pl

Laser Induced Breakdown Spectroscopy (LIBS) is one of the candidate methods for diagnostics of fuel retention and removal and wall composition in ITER. However, it is still questioned if its reliability and accuracy can meet the high requirements for diagnostics for the next-step fusion reactors. The main concerns lie in:

- the repeatability and quality of the spectroscopic signal in stable and well-defined conditions (i.e. power density of delivered laser beam, plasma parameters),
- behavior of the method for mixed material components, especially metals due to high number of spectroscopic lines of them,
- sensitivity of the method for thin layers which contain small amounts of fuel species

The experiment was carried out to assess the method for the laser treatment of ASDEX Upgrade (AUG) strike-point tiles and calibrated C:W:Al samples prepared by the Institute of Electronic Materials Technology (IEMT) in Warsaw. Two types of AUG samples were investigated: with 4 and with 200 μm tungsten coatings produced by PVD and VPS respectively on a graphite substrate. Most of the surface of the samples was in deposition zone where co-deposition/implantation of fuel ions is expected during AUG operation. The samples from IEMT were covered with ~3 μm layers with various calibrated mixes of C, W and Al (used as the Be analogue) by the means of sputter deposition.

In the experiment as an irradiation source a Nd:YAG laser system was applied. The laser delivered series of 3 ns, 0.6 J laser pulses at 1.06 μm with repetition rate up to 10 Hz. With the use of a lens the laser beam was focused to the diameter of about 3 mm at the target which resulted in the power density range of 10^8 W/cm^2. The applied spectrometer, Mechelle 5000 with iStar camera, made it possible to analyse the light in the wavelength range from 200 to 970 nm at wavelength accuracy of ±0.05 nm and the spectral resolution (λ/Δλ) of 4000. The spectrometer was used to record spectra of light emitted from the plasma generated in the vicinity of the laser-treated sample located in a vacuum chamber at ~$5 \cdot 10^{-5}$ mbar.

The presence of a deuterium line in LIBS spectra was recorded only for the first two laser shots in series for both types of samples. For the samples with thin coating, the most of tungsten was removed during the first 5 shots. The accumulated spectrum for the first two shots shows two distinct peaks of D/H alpha line and tungsten. It is worthwhile to note that the signal level for this shots is significantly higher than for the next shots, which suggests that LIBS investigation is convenient for detection of hydrogen isotopes even if they are trapped on the very surface of a laser-treated sample.

In the spectra of subsequent laser shots the tungsten lines become less significant due to removal of the layer and carbon lines which are below the detection level for the first two shots become dominant. For all samples, the magnitude of the deuterium line taken at the first laser shot was at the level of the highest tungsten line with ±30 % variation. In contrary to the high stability of the Dα line, the lines of tungsten have not shown good repeatability but in each spectrum there were a few lines of high magnitude. This problem may be attributed to the complexity of the spectrum, which consists of many lines. On the other hand, increasing of delay of the recording, the contribution of lines corresponding to W^{+1} and W^0 increased in comparison to W^{+2} lines. This phenomenon is consistent with the lower propagation velocity of this kind of particles.

A number of calibrated samples with different mixes of ITER relevant materials have been investigated with the use of LIBS in the same set-up as for the AUG samples. One of the goals of these investigations was to measure spectroscopic signals corresponding to carbon, tungsten and aluminum for different mixtures of these components. For this purpose the concept of “synthetic contents coefficient” (Scc) was developed. The synthetic contents coefficient was the indicator of the contents of the spectroscopic signal corresponding to a given element in the overall spectroscopic signal of all plasma components. The coefficient was calculated with the use of the formula: $S_{CC} = \Sigma I_{IE} / \Sigma I_{AE}$, where ΣI_{IE} is the sum of intensities of the representative lines of the element under consideration and ΣI_{AE} is the sum of all the representative lines in spectra. Table 1 shows a set of mean values and standard deviations of Scc obtained for the components of three different samples based on statistic calculations applied for the results obtained in 6 series of irradiation under the same experimental conditions (time delay 150 ns and gate 500 ns).

The values of the coefficient in the table are correlated with the ratio of the components in the mix, although the dependence does not seem to be straightforward. The standard deviation of the coefficients is in most cases lower than 10%, which suggests that the measurement method and its parameters are reliable.

Table 1 Synthetic contents coefficient for the components of the different mixtures

Sample Id.	C:W:Al ratio	Mean Value ± Std. Deviation		
		Scc_C	Scc_T	Scc_{Al}
VII	1:1:1	0,3689 ±0,0325	0,3704 ±0,0539	0,0953 ±0,0169
VIII	2:1:3	0,3863 ±0,0487	0,2249 0,0193	0,3334 ±0,0255
IX	3:1:2	0,4363 ±0,0190	0,1828 ±0,0163	0,2794 ±0,0359

Another experimental aim was to investigate the behavior of the H_α line during subsequent laser shots at samples with different material mixtures. As it had been expected, hydrogen line was quickly decreasing in intensity for all types of layers. The experimental results for samples VII, VIII and IX are presented in figure 1 where the obtained data points are shown together with the curves fitted to the exponential decay of the second order. The shapes of the fitting curves are very similar for all mixes, although, the fluctuation of data points, especially for the red line is visible. It suggests that LIBS diagnostics for measuring the contents of the hydrogen isotopes during the laser removal process may be relatively insensitive to the material mix of the layer in which retention takes place. The fluctuations observed for the red curve may be result from the local chemical nonuniformity of the layers which consists of materials with various hydrogen retention capabilities. To construe the results, one should also bear in mind, that total amount of the released hydrogen depends also on the removal rate of the layer.

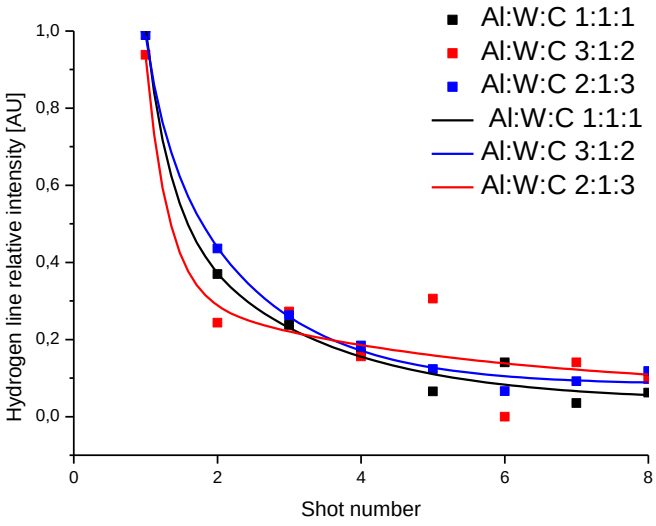

Fig.1 Experimental data for relative intensity of Hα line for layers with a different mix in dependence of the laser shot number and their fits

The results obtained for both, samples exposed in fusion devices and calibrated ones suggest that LIBS can be a very convenient method for detection and measurement of even small amounts of hydrogen isotopes released under laser treatment. The most important feature looks to be relatively independent from changes in the mix of the layer under investigation. In order to obtain good quantitative results still some experiments with precisely calibrated samples are needed, but reaching the goal is the issue of getting numerous results without further optimization of the method and calculative approach.

Quantitative analysis of the chemical contents of the samples by LIBS is a more demanding task due to the complexity of the spectra of metallic components and cross-correlations between their synthetic contents coefficients, nevertheless, the results presented in this paper suggest that correlations

between the amounts of the components and their content in the spectra are evident. Similarly as for quantitative measurements of the hydrogen isotope contents, further experiments on precisely calibrated samples are needed as well as analysis of the laser-treated surfaces by the means of materials research methods. These tasks are going to be a subject of the future experiments and studies at the IPPLM.

Assessment of the suitability of neutron and gamma detectors in the future experiment at JET for the validation of shutdown dose rate prediction

Corresponding author **Marek Scholz**
marek.scholz@ipplm.pl

At the shutdown of the machine, the decay gamma spectra outside vessel strongly vary with time after irradiation and tests on NaI and HPGe spectometers are in progress. Some primary tests showed that the NaI(Tl) detector cannot be used because of a poor energy resolution and also there are some problems with using a HPGe detector. The dewar appeared to be too heavy for mounting the detector in the desired upper port position. Furthermore, the detector cannot be left in the Torus Hall during the reactor operation because the germanium could be activated by neutrons. The BrilLanCe 380 and CdTe/CdZTe detectors could be used successfully in the proposed experiments. The BrilLanCe 380 detector is equipped with a scintillator made of $BrLaBr_3(Ce)$, it is relatively light (< 1 kg), compact, requires no cooling, and has apparently acceptable energy resolutions (about 1-2%). CdTe/CdZTe detectors are compact and do not require cooling with liquid nitrogen, with suitable electronics the energy resolution can achieve values of 1 % or better. Those have already been successfully utilized in conventional fission reactor activation diagnostics. Concerning dose rate measurements, besides the already used high sensitivity thermoluminiscent detectors, the BeO optically stimulated dosemeters could be employed for their good energy and dose range of linearity over more than six orders of magnitude.

The radiation spectrogram has been measured by two spectrometric systems. One of them consists of BiLanCe probe and appropriated electronics units as well as second based upon HPGe detector. The experimental setup is presented Fig. 1. On the foreground of picture are presented both spectrometric systems inside the PF-1000 device. On the background they are visible inner electrode made from cuprum and outer electrodes setup made for steel cylinders.

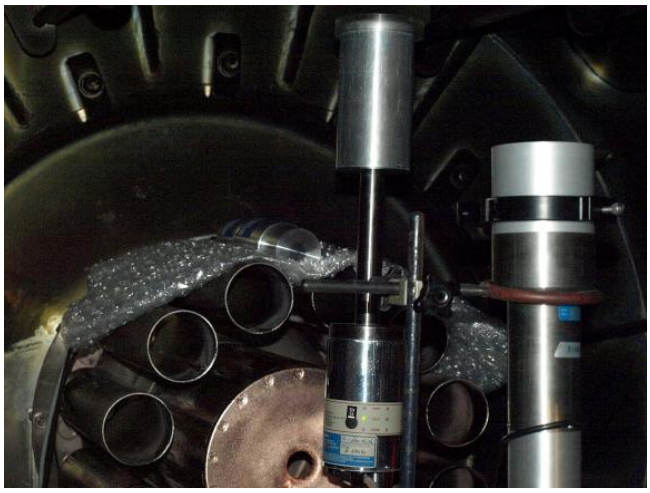

Fig. 1 The experimental setup consists of two spectrometers placed inside the PF-1000 device

In results of 80 hours of exposition of experimental spectrometers by the radiation inducted by neutrons inside the construction materials the radiation of the vacuum walls were measured. Fig. 2 presents the spectrogram collected by the BrLanCe probe. There are visible only some radiations peaks generated by activated radio-nuclides deposited inside the chamber walls.

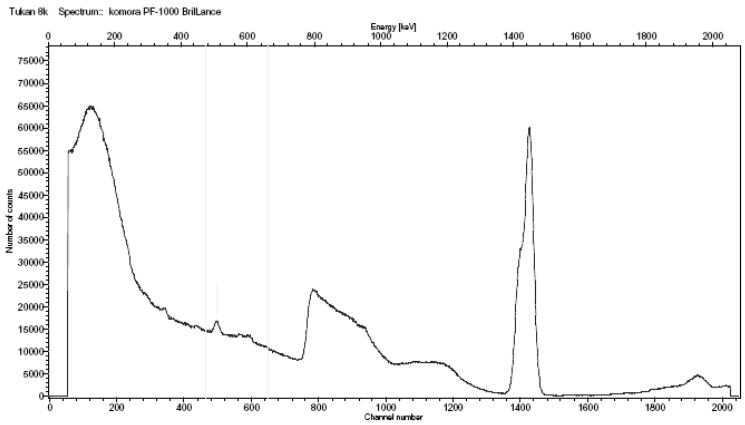

Fig. 2 Basic spectrogram obtained by means of BrilAnCe 380

Fig. 3 presented the spectrogram obtained with HPGe detector. The discrete structure of peaks allows discriminating all radiations emitted activation products inside the PF-1000 chamber from natural radiation background.

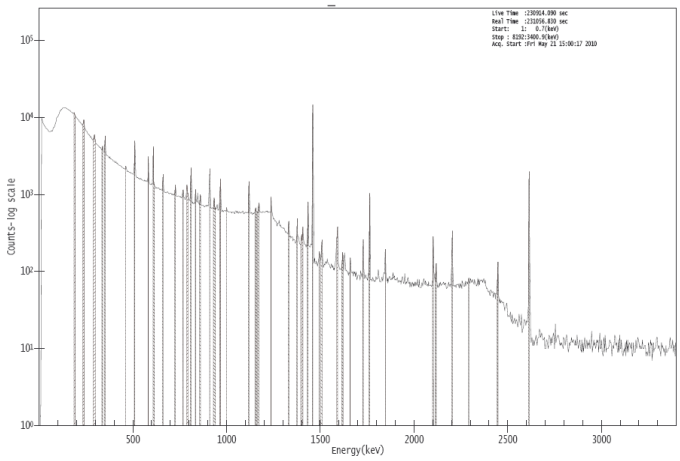

Fig. 3 Reference spectrogram obtained by means of HPGe system

In results of the spectrometric analyze the following nuclear reactions have been detected as results on neutron activation: Fe54(n,p)Mn54, Fe56(n,p)Mn56, Mn55(n,γ)Mn56, Mn55(n,2n)Mn54, Ni58(n,p)Co58, Ni58(n,2n)Ni57, Ni60(n,p)Co60,. The gamma emitted product of the above reactions would be the main source or radiation hazard after shut down of the device due to their long rand half time life period. The result can be summarized as follows:

- In results of a half a year of the d,d Plasma Focus operation several of radionuclides have been inducted inside the construction materials. Some of them was created by 14 Mev neutrons.
- The half live times of the above radionuclides have had a wide range from a few second up to many years.
- The hazarders of created radionuclidues becomes Co-60 because of its long half live time.
- The short term radiation risk becomes from wide range of short half time radionuclides.

- The BrLanCe probe has been calibrated by means of cross calibration method.
- The experimental setup dedicated for the above researches consists on BrLanCe probe with corresponding electronics TUCAN MCA analyzer and HPGe system for its cross calibration
- The advantage of BrLanCe probe manifests itself by relatively high efficiency of registration which dedicated it for long term studies.

MCNP simulation for JET 3U irradiation–end

Corresponding author **Marek Scholz**
marek.scholz@ipplm.pl

The measured neutron fluence at the irradiation point is related to the total neutron production by applying a calibration factor that is determined using neutron transport calculations (e.g., MCNP code), taking into account the geometry of the detector and the geometry and composition of the samples. Benchmark experiments, using suitable calibration neutron sources, must be performed to check the reliability of the calculations

The Monte Carlo neutron transport code – MCNP5 was applied to calculate the activation coefficients for the new materials used during recent JET campaigns. It allows the simulation of the influence of the real surroundings on the neutron flux and spectrum.

The activation coefficient (K) represents the probability of inducing the reaction (the number of reactions per target nucleus per source neutron). A neutron transport code MCNP is usually used to calculate the activation coefficients for the different activation materials.

The original input file for MCNP represents the simplified geometry and materials of the JET structure, and was elaborated by M. Loughlin et al. The considered model includes a D-D neutron source only and does not take into account the triton burn-up reaction. The original model contains only some details of the irradiation point (3U IE) surroundings. The model did not include the cooling water used with the 3U IE. To analyse the influence of the cooling system and other nearby structures on the neutron energy spectrum, we improved the representation of the nearest surrounding region in the MCNP model (see Fig. 1).

The neutron energy spectrum calculated using the MCNP code, which takes into account the above-mentioned complement, is compared in Fig. 2 with the spectrum calculated without this complement. The 10^9 MNCP histories were carried out for each of the considered configurations.

One can see that the alterations of the input geometry result in the change of the calculated spectrum. The differences are observed in the thermal as well in the fast neutrons regions. The adapted MCNP input file was then used to calculate the activation coefficients for the materials applied in our experiments performed during C20 – C27 Experimental Campaigns at JET. The obtained activation coefficients allow us to link the measured activities to the total neutron yield, and they could also be used for the energy spectrum deconvolution.
There is a small discrepancy between the activation coefficients for the ^{115}In(n,n') reaction calculated using MCNP by our group with original input ($4.02 \cdot 10^{-31}$) and by M. Loughlin et al. ($4.03 \cdot 10^{-31}$). This difference may result from the different cross-section libraries used in the calculations. One should remember that the experimental activation coefficients are estimated employing JET neutron diagnostics, which had been previously cross-calibrated using the coefficients.

It should be noted that the calculated activation coefficients may change when using other cross-section libraries. In spite of that, one can see, that applying the results of the calculations for improved geometry causes decrease of the activation coefficients.

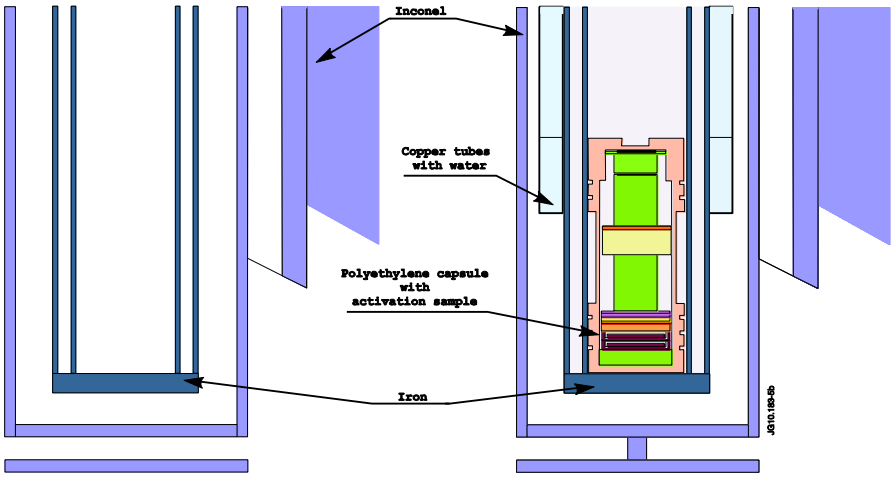

Fig. 1 Comparison of the original and supplemented geometry of the 3U IE applied to the MCNP calculations

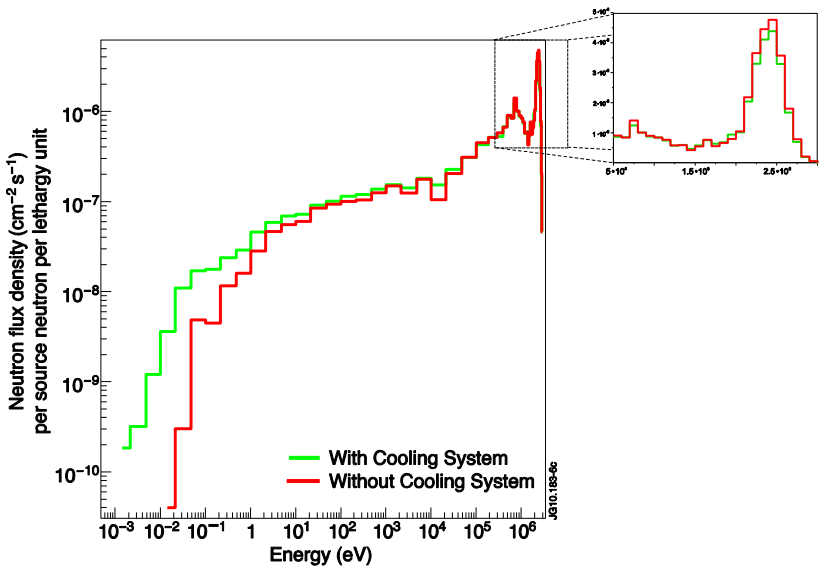

Fig. 2 MCNP-calculated neutron spectrum at 3U IE with and without consideration of the cooling system

Particularly significant is the fact that the new geometry gives for the ^{115}In(n,n') reaction an activation coefficient 11% lower than the predicted one using the old geometry. This result, if confirmed by further necessary analysis, can affect noticeably the 2.5-MeV neutron yield determination at JET as the ^{115}In(n,n') reaction is used to cross-calibrate other diagnostics, especially neutron monitors (KN1).

These results indicate that real neutron spectrum in 3U IE is more thermalised than is suggested by the original MCNP calculations, but quite as much as it is resulted from the supplemented calculations. The results of the improved calculations for the radiative capture reaction of Al, In, and Au suggest a correct restoration of the thermal neutron spectrum, whereas the calculations for Y and Co do not. These results mean that a more careful reconstruction of the closest surrounding of irradiation point should be performed in the MCNP simulations because it influences the results of the activation coefficients calculation.

Gamma Ray Cameras: Neutron Attenuators

Corresponding author **Marek Scholz**
marek.scholz@ipplm.pl

The JET KN3 gamma-ray cameras diagnostics system has already provided valuable information on the fast ion evolution in JET plasma. The applicability of gamma-ray imaging diagnostics to high power deuterium pulses and to deuterium-tritium discharges is strongly dependent of the fulfilment of rather strict requirements for the control of the neutron and gamma-ray radiation fields. One of the objectives consists in the design, construction and testing of neutrons attenuators for the vertical and horizontal cameras of the KN3 gamma-ray imaging diagnostics. This diagnostics upgrade should make possible gamma-ray imaging measurements in high power deuterium JET pulses, and eventually in deuterium-tritium discharges. All the components of the KN3-NA assembly have been manufactured and tested on a test stand which is an exact replica of the KN3 horizontal camera neutron attenuator assembly and partially replicates the installation configuration for the KN3 vertical attenuator installation configuration. Mechanical, electrical, pneumatic and hydraulic tests were performed. The next step for the validation of the KN3-NA system consisted in radiation tests. These tests were performed by using the PF-1000 plasma-focus device at IPPLM.As it is not possible to test the attenuators at their final location, using the KN3 detectors, an independent setup was planned in order to get experimental info on the neutron field. This setup includes the use of other detectors than those of the KN3 diagnostics. The experiments have to be compared with MCNP calculations. A key point is represented by the attenuation factor. The experiments should prove that the value of the attenuation factor is in agreement with the value estimated to be attainable within the project constraints (see Table 1).

Table 1

Neutron attenuator	Material	Neutron energy	
		2.45 MeV	14.1 MeV
KN3-HC-NA	H_2O	10^2	15
KN3-VC-NA (Long)	H_2O	10^4	10^2
KN3-VC-NA (Short)	H_2O	10^2	15

In order to measure the transfer function of attenuator, the neutron field was measured using super-heated fluid detectors, SHFFD's (also known as "bubble detectors"). SHFD are suspensions of metastable droplets which readily vaporize into bubbles when they are nucleated by radiation interactions. The active detecting medium is in the form of microscopic (20-50 μm) droplets suspended within an elastic polymer. For a standard bubble detector like the BD-PND type, the energy response is approximately flat within the range 0.3-10 MeV.

Using detectors with different energy thresholds, a bubble detector spectrometer (BDS) is obtained. The BDS covers a broad energy range (0.01 – 20 MeV) and provides six energy thresholds in that range (Fig. 1). Therefore the SHFD detectors were be used for measuring the neutron fluence and also to determine the energy spectrum. The detectors were placed inside a paraffin collimator in order to ensure additional shielding.

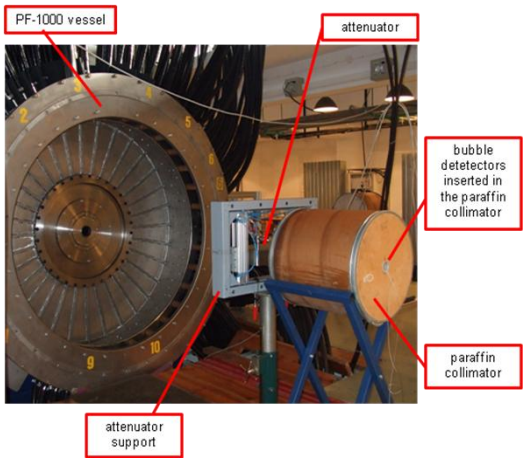

Fig. 1

In order to test this configuration neutron spectra were recorded, using detectors with the energy thresholds listed in Table 2 (BDS bubble detector spectrometer). It worth to be mentioned that for these experiments new spectrometric detectors (BDS), with increased efficiency and energy threshold above 1 MeV were purchased and used.

Table 2 BDS energy thresholds/energy bins

BDS spectrometer for energy distribution recording - energy thresholds/energy bins (MeV):	BDS energy bins used for attenuation factor determination (MeV)
• 0.01-0.10 • 0.10-0.60 • 0.60-1.00 • 1.00-2.50 • 2.50-10.00	• 1.00-2.5 • 2.50-10.00

The attenuation factor was determined by recording the detector response, with and without attenuator, in the energy range above 1 MeV. The detectors were exposed to multiple shots in order to ensure a good statistic. The total neutron production was 0.81×10^{12} for the measurements without attenuator and 1.03×10^{12} for the measurements with attenuator respectively. The detector responses were scaled in respect with the neutron production characteristic during their exposure and also according to their sensitivity. The detector response function was used for detector response deconvolution. The evaluation of the attenuation factor is summarized in Table 3.

Table 3 Attenuation factor evaluation

Geometry	Total neutron production	Coorected no of bubbles	Factor
Without attenuator	$0.807\ 10^{12}$	88 ± 1.43	112 ± 31
With attenuator	$1.032\ 10^{12}$	0.79 ± 0.43	

The evaluated attenuation factor proved to be in agreement with the attenuation factors considered to be attainable within the project constraints (~ 10^2).

Gas Electron Multiplier Detector for X-ray Crystal Spectrometry – GXS

Corresponding author **Marek Scholz**
marek.scholz@ipplm.pl

The motivation for the upgrade of the KX1 diagnostic was discussed in details in PMP report [4]. Here we present only main conclusion from this report. The necessity of the exchange of the detector is related to the fact that the previous gas x-ray detector has been damaged and not been operated since 2008/2009. Moreover, the ITER-oriented JET research program brings a new important requirement for the KX1 diagnostic which is expected to monitor the impurity level of Tungsten – the main component of a new JET ITER-like divertor. Therefore besides the upgrade of the Ni monitoring diagnostics, in order to implement the W impurity monitoring one has to design and construct a new diagnostic channel based on the same KX1 geometry.

A new diagnostic channel will operate with an additional (1011) quartz crystal (2d=6.68 Å) mounted in June 2009 and sharing the same 266 mm diameter beamline. The quartz crystal will be used for the reflection of low energy X-ray photons emitted by W^{46+} at 2.4 keV. The higher energy range of the W^{46+} spectra can be measured by means of the Si crystal which has been provided together with a new quartz crystal and can be curved and installed at a later time.

It should be noticed that in the case of the low x-rays energy (below 3 keV) the high transmission losses of the KX1 system (strong absorption in window materials) can significantly influence on the x-ray photon attenuation occurring in passive material of the detector and in this way strongly deform the measured spectrum. This makes hardly possible measurements with low amplitude threshold in the case of fast solid-state detectors. In the case of gas detectors low-energy x-ray lines emitted by the working gas (fluorescence, Auger electrons) may cause non-proportional relation between x-ray energy and signal amplitude. Therefore in the case of low-energy photons, the experimental data can be precisely recorded only in one main order of reflection (e.g. 2.4 keV), whereas the data from the other ones (4.8 keV or 7.2 keV) can be affected by an additional systematic error.

The present report is structured as follows. First, we define the prototype objectives and aims. Secondly, the detailed simulations of the optimal x-ray conversion layer and filling gases for maximum detection accuracy and efficiency for the both (low- and high-energy) prototype x-ray detectors are presented. Then, we present the technical description of the prototype GEM detectors and prototype electronics for GEM detectors. Finally, a short summary and outlook are given.

The conceptual design of the position sensitive gaseous x-ray detector for KX1 diagnostics was driven by the following assumptions/considerations:

- High conversion yield of 2.4 keV and 7.8 keV photons in the detector drift/conversion volume,
- Possibility of the relatively efficient registration of x-ray spectra in first, second and higher reflection orders,
- Full detection efficiency of photons converting in the drift/conversion volume,
- High detection rate capability,
- Dynamic range allowing good linearity in the wide x-ray energy range,
- Low rate of violent spontaneous discharges caused by highly ionizing background,
- Position resolution better than 0.5 mm in one dimension (1-D reconstruction),
- Robustness of the construction,
- Safe and environmentally neutral gas mixtures as a detection medium.

The choice of the suitable technique has been focused on Gas Electron Multiplier (GEM) technique as amplification structure in gas proportional counter with strip readout (1-D position sensitivity). As it was demonstrated by others, GEM structures may be organized in cascade thus allowing sequential charge amplification. Such a feature opens the possibility to obtain high charge gain with reduced probability of spontaneous discharges induced by alpha-particles. Accidental discharges may be destructive for the detector itself and for charge preamplifiers in the read-out chain. They also cause the detection dead-

time what should be avoided as the detector should be fully operational during the whole JET plasma discharge. The most suitable Micropattern Gas Detector structure for the task to be performed in KX1 is the Tripple GEM (T-GEM) geometry (Fig. 1).

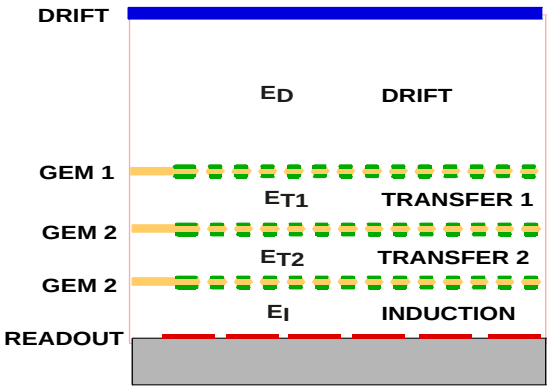

Fig. 1

The structure of the single prototype detector will be following:

- Cascade of 3 GEM foils with the gap 2 mm and 2.5 mm between each detector, respectively,
- Conversion gap of 15 mm with possibility to increase it by adding additional spacers,
- Readout plane with 0.8 mm strip pitch (128 strips in each detector),
- Induction gap width of 2.5 mm and 3.0 mm in each detector respectively,
- Mylar window with thin aluminum layer on the inner surface.

Analogue signals from strips will be transmitted via special SMD connectors to the back-plane serving to connect individual amplifier/shaper channels. The shaping constant of FEE will be tuned to match characteristics of the primary strip pulse and sampling rate of digitization in the Flash ADCs. As the precise analysis of cluster size and cluster amplitude is fundamental for position resolution and energy reconstruction to be achieved in the detection unit, great attention will be devoted to the optimization FEE and the strip plane structure.

Impurity production from the ICRH antennae in JET

Corresponding author **Agata Czarnecka**
agata.czarnecka@ifpilm.pl

Additional heating systems can be a source of impurities in fusion plasmas. Studies of impurity behaviour are important to understand and minimize their effects on tokamak plasma performance and for the design of future heating systems such as the ones foreseen for ITER. The Ni impurity release by the two ICRH antenna types in JET: the so-called ITER like antenna (ILA) and the A2 antennas has been monitored. Recently, a novel spectroscopic technique for the routine impurity analysis of plasma discharges, which accounts for the impact of impurity transport and electron temperature on the impurity density, ΔZ_{eff}, and plasma dilution have been established. The Ni impurity concentration have been studied through the detection of the Ni lines, by VUV spectrometer, known at JET as the KT2 diagnostic. Statistical techniques are used to derive global trends of the impurity content versus different independent variables.

The aim of the ITER-like antenna is to demonstrate coupling of Ion Cyclotron Resonance Heating (ICRH) power to plasmas in conditions at power densities and RF power levels relevant to ITER. In this context, it is very important to check what extent the large antenna power densities, characteristic of the compact strap array used in the ILA design influence the metallic impurity content in the plasma. The

results of this analysis are to be compared with the ones that have been obtained for the already existing A2 antennas (see fig.1). Such a comparison of two different antenna systems can contribute to answering the engineering question of maximizing the coupled ICRH power while minimizing the impurity content of the plasma.

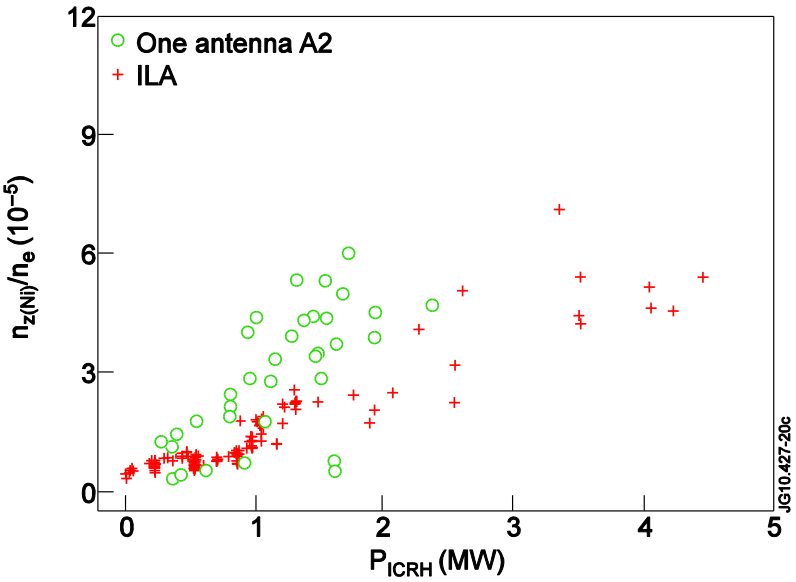

Fig. 1 Comparison of Ni concentration ($r/a \approx 0.5$–0.6) during the operation of the full ILA (crosses) and one A2 antenna (open circles) as a function of the launched ICRH power. The provided data points are time averaged over selected time windows where the plasma remained in steady state

It is very clear that for the same total power — but at a much higher power density up to 6.2 MW/m^2 — the ILA performs very well, with a low release of impurities into the core plasma in comparison with the A2 antennae.

To demonstrate the effect of different relative phasings of the antenna straps on impurity production, dedicated experiments have been undertaken in JET. Changing the relative phasings between the four straps of the A2 antennas modifies the spectrum of the parallel wave number $k_{||}$, resulting in different ICRH absorption by the plasma. Fig.2a shows the correlation between Ni concentration and total applied heating power for the different A2 antenna phasings, and Fig.2b shows the Ni content as a function of $k_{||}$ for pulses with the same plasma conditions and same ratio of NBI to ICRH power. It was observed that for antenna phasings with higher dominant $k_{||}$, the Ni impurity concentration was reduced in the central part of the plasma. The above results support the fact that for low absolute values of $k_{||}$ the heating efficiency is low, and the fraction of the total ICRH injected power that is not absorbed in the plasma core remains in the edge, thus contributing to increase the radiation losses. This behaviour can be related to a lower electric field on the antenna structure — the main source of Ni is thought to be the acceleration of edge particles in the antenna near field toward structures close to the antennas. The local mechanism responsible for the impurity influx from the antenna is the formation of RF enhanced sheaths along the magnetic field lines that intersect the Faraday Screen or the side limiters of the antenna. This leads to an acceleration of ions to the energies required for substantial sputtering.

The impurity content has also been monitored in experiments aiming at improving the ICRH coupling at large antenna strap–separatrix distances, up to 19 cm, by injecting deuterium (D_2) from different gas inlets in order to bring the fast wave cut-off layer closer to the antenna. It can be observed in Fig.3 that the Ni concentration decreases with increasing values of the ROG, and it also decreases with the D_2 injection rate.

The Ni concentration as a function of the D_2 injection rate from different GIM locations is presented in Fig. 4. The Ni content is reduced by injecting D_2 gas with the best results obtained with injection from the midplane or top of the tokamak. The contribution to Z_{eff} of the Ni impurity generated directly from the ICRH antenna is small and decrease with increasing gas puff rate. The relative changes observed in the Ni concentration, in both the ITER-AT and HT3 configurations, are larger than the relative changes in Z_{eff} , when changing the gas injection rate. It should be noted, that in JET the main impurity contributing to Z_{eff} is carbon released from the first wall. This can explain the behaviour of Z_{eff} and suggests that the effect of gas puff on impurity release is local to the antennas. The decreasing of the plasma dilution due to the Ni impurity as a function of the D_2 has also been observed.

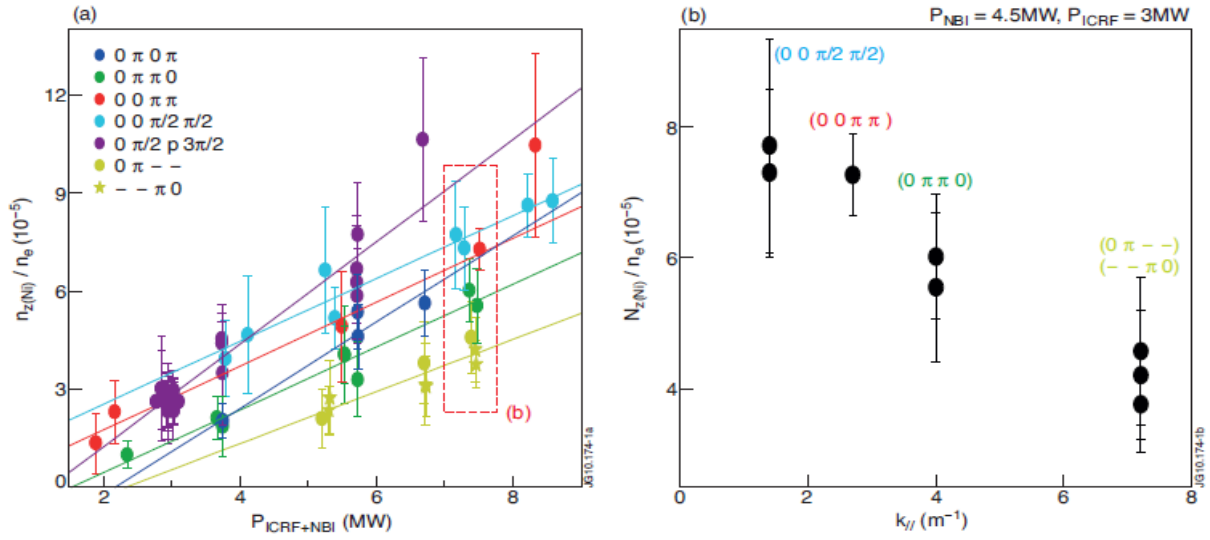

Fig. 2 a) Correlation between the Ni concentration (r/a ≈ 0.5–0.6) and total applied heating power for different A2 antenna phasings tested in 2009, and b) Ni concentration vs. parallel wave number $k_{||}$ for the points in the dashed box in a) with 3 MW of ICRH and 4.5 MW of NBI power

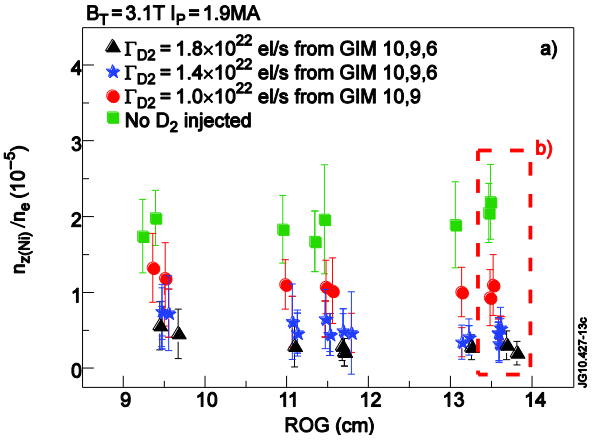

Fig. 3 Correlation between Ni concentration (r/a ≈ 0.5–0.6) and antenna–separatrix distance ROG (ITER-AT configuration)

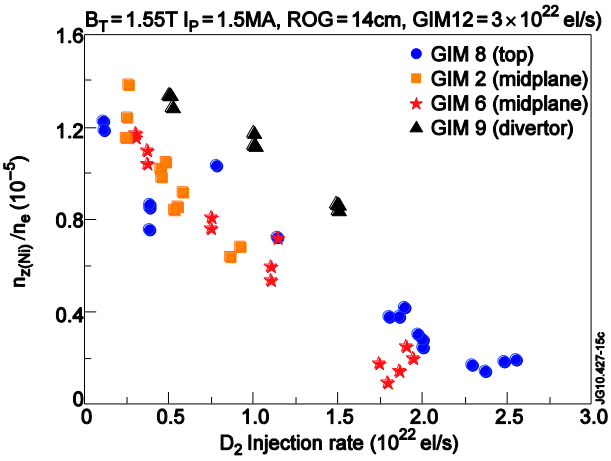

Fig. 4 Effect on Ni concentration (r/a ≈ 0.5–0.6) of D_2 gas injection using different GIMs (HT3 configuration).